Chemical Engineering Journal 489 (2024) 151390

Contents lists available at ScienceDirect

Chemical Engineering Journal

journal homepage: www.elsevier.com/locate/cej

# Decipher syntrophies within C2-C4 organic acids-degrading anaerobic microbiomes: A multi-omic exploration

Gabriele Ghiotto [a,1], Anna Detman-Ignatowska [b,1], Aleksandra Chojnacka [b,c], Esteban Orellana [a], Nicola de Bernardini [a], Sofia Fraulini [a], Laura Treu [a,*], Anna Sikora [b,2], Stefano Campanaro [a,2]

[a] Department of Biology, University of Padua, via U. Bassi 58/b, 35131 Padova, Italy
[b] Institute of Biochemistry and Biophysics Polish Academy of Sciences, Pawinskiego 5a, 02-106 Warsaw, Poland
[c] Department of Biochemistry and Microbiology, Institute of Biology, Warsaw University of Life Sciences-SGGW, Building 37, Nowoursynowska 159, 02-776 Warsaw, Poland

ARTICLE INFO

*Keywords:*
Anaerobic digestion
Flux balance analysis
Genome scale metabolic modeling
Machine learning functional prediction
Metatranscriptomics

ABSTRACT

In methanogenic ecosystems, carboxylic acid degradation is a crucial process facilitated by specialized bacteria working in syntrophy with methanogens. This study explores the transcriptomic responses in 178 metagenome-assembled genomes upon changes in feeding composition, specifically lactate, butyrate, propionate, and acetate, in four lab-scale bioreactors. *Methanothrix soehngenii* and *Methanoculleus* sp. emerged as key biomethanation contributors. Through metatranscriptomics, machine learning-based functional annotation, and flux balance analysis the underlying microbial interactions and dynamics were deciphered. *Syntrophomonadaceae* and *Mesotoga* species maintained mutualistic metabolite exchanges with hydrogenotrophic methanogens, degrading primarily butyrate and lactate, respectively. Acetate was mainly consumed by *Smithellaceae* sp., in competition with *M. soehngenii* in all reactors. Furthermore, the acetoclastic archaeon exhibited a previously undocumented capability to metabolize lactate, thereby confirming the prevalence of acetotrophic pathway. Transcriptomic profiles revealed an additional layer of complexity, where propionate dismutation and beta-oxidation pathways are interconnected by the exchanges of butyrate between putative syntrophs, including *Syntrophomonadaceae* and *Smithellaceae* species. Integrating multi-omics data with genome-scale metabolic modeling enabled the accurate reconstruction of dynamics within the controlled ecosystem. This composite novel approach was applied to the AD system to unveil the intricate relationships operating within the microbiome to promote thriving. Results elucidated the still poorly explored organization of the so-called microbial dark matter.

## 1. Introduction

The increasing awareness of climate change and greenhouse gas emissions has spurred research efforts to enhance biofuel and bioenergy production while reducing reliance on fossil fuels. Residual biomass and by-products offer opportunities for effective renewable energy generation through anaerobic digestion (AD) [1,2]. Governed by a complex microbiome [3], AD transforms organic carbon into carbon dioxide ($CO_2$) and methane ($CH_4$) through four sequential steps: hydrolysis, acidogenesis, acetogenesis, and methanogenesis. The latter is exclusively mediated by anaerobic archaea, using either acetate, hydrogen ($H_2$) and $CO_2$, or methylated C1 compounds as substrates. These intermediate metabolites result from the acetogenic step, through the degradative activity of carboxylic acids-oxidizing bacteria [4]. The strong interconnections between acetogenesis and methanogenesis, driven by syntrophic associations between acetogenic bacteria and hydrogenotrophic methanogens (HM), render the process thermodynamically favorable. Organic acid oxidation involves various microbial guilds capable of exploiting substrate-specific metabolisms [5]. Butyrate is processed through beta-oxidation by microbes such as *Syntrophomonas*

*Abbreviations:* AD, Anaerobic digestion; FBA, Flux balance analysis; GEMs, Genome scale metabolic models; HM, Hydrogenotrophic methanogens; ML, Machine learning; WL, Wood–Ljungdahl.

* Corresponding author.
*E-mail address:* laura.treu@unipd.it (L. Treu).

[1] These authors contributed equally to this work.
[2] These authors also contributed equally to this work.

https://doi.org/10.1016/j.cej.2024.151390
Received 26 January 2024; Received in revised form 28 March 2024; Accepted 16 April 2024
Available online 16 April 2024

*wolfei* [6] and *Syntrophus acidotrophicus* [7]. For propionate, there are two main pathways: the methylmalonyl-CoA pathway, observed in *Syntrophobacter* species [8], and the dismutation pathway found in *Smithella propionica* [9]. Acetate instead is primarily processed via the Wood–Ljungdahl pathway (WL), as already demonstrated in *Syntrophaceticus schinkii* [10]. This pathway can function bidirectionally, enabling acetyl-CoA production from $CO_2$ through diverse electron donors, or serving as an electron sink during carbohydrate or organic acid fermentation [11]. However, not all acetate-oxidizing microbes can exploit both directions of this route. Additionally, the glycine synthase-reductase (GSR) pathway has been proposed as an alternative route to the WL pathway [12]. In this case acetate undergoes conversion to acetyl-CoA, leading to the generation of glycine, ultimately resulting in the production of two methylene-THF molecules through the glycine cleavage system (GCS). Furthermore, studies on *Acetobacterium woodii* revealed how oxidation of lactate to acetate occurs through a complex formed by the FAD-dependent lactate dehydrogenase and the electron transfer flavoprotein [13,14]. Altogether, these diverse metabolic routes play a crucial role in establishing and maintaining syntrophic associations, ensuring an efficient and balanced conversion of carboxylic acids within anaerobic environments, as previously demonstrated [15]. However, mutually symbiotic relationships occurring between microbes, remain largely unexplored, partially due to the difficulties in following the intricacy of metabolic exchanges occurring. Metagenomics alone cannot offer a sufficiently detailed understanding of the diversity and dynamics of methanogenic processes. Therefore, validation through transcriptome-level analysis is essential to obtain a comprehensive picture of microbiome behavior [16–18]. In our previous study, metagenomics, stable carbon isotope of fermentation gas, and bioreactor performance monitoring were employed to characterize the microbiome of four Up-flow Anaerobic Sludge Blanket (UASB) reactors [19]. Although all bioreactors exhibited similar $CH_4$ production rates, isotopic analyses highlighted that acetate and lactate favored the acetotrophic pathway, while hydrogenotrophic methanogenesis was preferred when butyrate and propionate were provided as substrates [19]. To validate these findings, the current study employs a combined multi-omics approach to investigate the same microbiome, integrating transcriptomic data into genome-scale metabolic models (GEMs) and flux balance analysis (FBA). These mathematical representations successfully revealed bioconversion abilities, growth requirements and inhibitor susceptibility of microbes [20–22]. Acetogenesis and methanogenesis complexity during lactate, butyrate, propionate and acetate processing were unraveled by valuable metatranscriptomics insights and the precise reconstruction of metabolites exchanges, corroborating and expanding prior findings [19]. Results were further validated through supervised machine learning (ML), which has been extensively employed in the biological field to model complex interactions and investigate the intricate links between genotypes and phenotypes. In particular, the functional capabilities of organisms were predicted from their KEGG gene annotation using supervised machine learning, an approach that was proven to be successful in the functional classification of organisms according to their genetic content [23,24]. The effectiveness of multi-omic analyses in reconstructing the intricate puzzle of microbial dynamics and metabolic roles within bioreactors was showcased, addressing future perspectives from recent syntrophies investigation [25] and offering promising avenues for optimizing $CH_4$ production.

## 2. Materials and Methods

### 2.1. Experimental setup and analytical methods

Four methane-producing anaerobic microbial communities, were cultivated in 3.5-liter UASB bioreactors at mesophilic conditions (21–23 °C), utilizing synthetic media designed to simulate a blend of non-gaseous byproducts from various acid fermentations, with a predominant emphasis on lactic (M1), butyric (M2), propionic (M3), or acetic acid (M4). The original methanogenic inoculum derived from anaerobic activated sludge collected from the "Warszawa Południe" municipal waste treatment plant in Warsaw, Poland. The UASB bioreactors were operated for 886 days (Fig. S1). In the first 667 days, substrate adaptation and process stabilization were done to establish substrate-specific microbiomes. Five media compositions were tested during this period (Fig. S1, Table S1) and the main carbon sources were the same used in Experiment 1 for each reactor (Table S2). In Experiment 1, carbon and energy sources varied (Table S2). Specifically, for M1: sodium lactate (10.71 g/L), sodium butyrate (1.30 g/L), propionic acid (0.96 g/L), and acetic acid (0.96 g/L); for M2: sodium lactate (1.3 g/L), sodium butyrate (9.0 g/L), propionic acid (0.96 g/L), and acetic acid (0.96 g/L); for M3: sodium lactate (1.30 g/L), sodium propionate (9.0 g/L), butyric acid (0.94 g/L), and acetic acid (1 g/L); for M4: sodium lactate (1.3 g/L), sodium acetate trihydrate (9.8 g/L), butyric acid (0.94 g/L), and propionic acid (0.96 g/L). In Experiment 2, each medium contained a single dominant component: 15.3 g/L of sodium lactate (M1), 12.8 g/L of sodium butyrate (M2), 12.8 g/L of sodium propionate (M3) and 17 g/L of sodium acetate trihydrate (M4). Starting from day 17 the respective media were supplied to the UASB bioreactors using a peristaltic pump such that the hydraulic retention time was 7 days, with a resulting upflow rate of 0.5L/day. Prior to Experiment 1 and Experiment 2, there were periods of 9 and 47 days, respectively, with the medium flow turned off to reduce concentrations of organics with unknown $^{13}C$ isotope content. Throughout the operation, physicochemical parameters, including pH, COD, biogas production rate, and gas composition ($CH_4$ and $CO_2$), were monitored (Table S4,S5). Additionally, stable carbon isotope analyses and volatile fatty acids (VFA) were assessed in biogas and effluent samples from Experiments 1 and 2 (Table S6-S8). On the 751st and 884th days of operation, methanogenic sludge samples were collected for DNA and RNA analyses, marking the end of Experiment 1 (days 710–751) and Experiment 2 (days 799–884). Extended details about experimental setup and analytical methods are reported in a previous publication [19].

### 2.2. Total RNA isolation and sequencing

Triplicate samplings were conducted independently throughout the entire bioreactor, employing a glass pipette with a fractured tip. Subsequently, the sludge was promptly frozen in liquid nitrogen. RNA isolation and sequencing were executed separately for each technical replicate. Total RNA purification was accomplished using the RNeasy PowerSoil Total RNA Kit (Qiagen). Approximately 1 g of samples was utilized for RNA isolation, and the isolated RNA was stored at −80 °C. Prokaryotic ribosomal RNA was eliminated using the RiboZero Universal Bacterial rRNA Removal Kit (Illumina, San Diego, USA). Construction of cDNA libraries was performed using the KAPA Stranded RNA Seq kit (KAPA-Roche, Basel, Switzerland), following the manufacturer's protocol. Quality and quantity of purified libraries were assessed using the Agilent 2100 Bioanalyzer, Qubit®2.0 (Life Technologies, Thermo Fisher Scientific, Waltham, USA), and the KAPA Library Quantification kit (KAPA-Roche, Basel, Switzerland). Subsequently, libraries were sequenced on Illumina NextSeq 550 with 2 × 75-bp paired-end reads, resulting in a sequencing depth between 45–90 million reads, depending on the sample. Raw DNA and RNA sequences generated, have been archived in the SRA with accession codes PRJNA680596 and PRJNA1052968, respectively.

### 2.3. Metagenomics, gene-level and machine learning investigation

An updated genome-centric metagenomic pipeline was employed to retrieve microbial genomes [26], enhancing the results of the prior study by integrating additional binning software and a refinement step. DNA libraries were sequenced on Illumina NextSeq 550 with 2 × 150-bp paired-end reads, with a sequencing depth between 40–100 million

reads, depending on the sample. The sequencing reads underwent preprocessing using Trimmomatic v0.39 [27]. To check for contamination, BBDuck v38.93 [28] was utilized. Paired reads were merged with BBMerge v38.93 [28], and short-read co-assembly was conducted using Megahit v1.29 [29], resulting in an assembly size of 4.06 Gb. The Metagenome-Assembled Genome (MAG) acquisition involved multiple binning software: MaxBin v2.2.7 [30], MetaBAT1 [31], MetaBAT2 v2.15 [32], and VAMB v3.0.2 [33]. Subsequently, MAGs were refined and dereplicated utilizing DAS_Tool v1.1.6 followed by dRep v3.4.0 [34]. Only medium to high-quality MAGs were retained for subsequent analyses, according to MIMAG standards [35]. Quality and completeness of MAGs were evaluated using checkM2 v1.0.2 [36], and their relative abundance (RA) was estimated through coverM v0.6.1 [37] (Table S5). Taxonomic assignment was carried out using GTDB-TK v2.1.1 [38] and database version R214. Phylogenetic tree was built using PhyloPhlAn v3.0 [39]. Gene prediction was executed using Prodigal v2.6.3 [40] and functional annotation with eggNOG-mapper v2.1.10 [41]. The KEGG database [42] was used for manual metabolic reconstruction of pathways of interest (Fig. S2). A ML classifier predicting butyrate oxidizers was implemented, training the model with logistic regression, random forest, and support vector machines algorithms (Supplementary Methods).

### 2.4. Genome-centric metatranscriptomics

RNA-seq reads underwent preprocessing with Trimmomatic v0.39 [27] and were aligned to the MAGs using Bowtie2 [43]. RPKM profiles for the reconstructed MAGs were computed with coverM v0.6.1 (Table S5). The correlation between biochemical parameters, RA and RPKM was visualized through a Principal Component Analysis (PCA) using the envfit() package (Table S6-S7, Fig. S3). HTSeq v2.0.2 [44] was utilized to count the number of RNA fragments per gene in stranded mode. For transcriptome data analysis DESeq2 v3.14 [45] was employed. Each MAG was processed independently, excluding genes with a cumulative count across all samples of 5 or fewer. The remaining normalized counts were then transformed into a $\log_2$ scale. Differential expression analysis with DESeq2 [45] was defined using the design formula "Reactor + Timepoint". For each reactor, the $\log_2$ fold change ($\log_2$FC) was calculated by comparing the gene expression on day 884 (TP2) with that measured on day 714 (TP1). Analysis was conducted employing a Wald test and a false discovery rate threshold of 0.05, along with a $\log_2$FC threshold of 1. Furthermore, fragment counts were normalized separately for each MAG. Size factors were calculated using the Estimate Size Factors function [45] and applied to raw counts, resulting in normalized counts. These were normalized by gene and scaled by a factor of $10^3$, resulting in Fragments Per Kilobase (FPK) values (Supplementary Methods). Downstream analyses were performed only on a subset of MAGs, satisfying the threshold of 5 RPKM in at least one RNA sample (Table S5, Fig. S4). A PCA was performed on the RPKM profiles of the selected MAGs to evaluate the difference in activity level depending on the carbon substrate (Fig. S5). A gene-level investigation was then performed on genes involved in methanogenesis (hydrogenotrophic and acetoclastic) and carboxylic acid oxidation (lactate, butyrate, propionate and acetate). Genes were selected according to literature information (Fig. S6). The mean of the resulting FPK values was calculated from the sample triplicates, in order to display only the average FPK in Figs. 2-3 and Tables S8-S9.

### 2.5. Flux-balance analysis and metabolic modeling

MAGs with RA exceeding 1 % were chosen for in silico metabolic modeling reconstruction. GEMs were built from MAGs using gapseq v.1.1 [46], selecting the most suitable metabolic reaction database and applying default gene matching parameters to restrict the search within taxonomic boundaries. Draft GEMs were constructed, and when sufficient taxonomic information was accessible, biomass reactions were specified. When such information was lacking, automatic inference was employed. Default parameters governed the use of bit score thresholds (−l and −u) to categorize reactions with or without sequence evidence. Subsequently, utilizing Micom (v.0.10.1) [47], species-specific GEMs were manipulated to construct a unified model that concurrently considers the exchange fluxes between individual species and between the collective microbiome and the environment. Community-level constraints were established by considering supplied feedstock and measured VFA. Dry weight approximations and total culture volumes were utilized to calculate rates, expressed in mmol/g/h. FBA was conducted, with the microbiome biomass accumulation set as the objective, using a cooperative trade-off approach (equal to 0.7). RNA information was used to create Condition-specific Communities (CoCo-GEMs) as previously described [48]. The RA of various species were incorporated to account for community composition (Supplementary Methods, Fig. S7-S10, Table S11-S15).

## 3. Results and discussion

### 3.1. Metagenomic reconstruction of complex AD system

The anaerobic microbiota was systematically investigated in relation to various feeding substrates. By employing assembly-based multiple binning approaches a total of 178 medium-to-high quality MAGs were reconstructed (Table S5). To gain deeper insights, the dominant fraction of the microbiome, encompassing 21 species with RA exceeding 1 % (Fig. 1), was investigated. Two methanogenic species were predominant, *Methanothrix soehngenii* MB13 and *Methanoculleus* sp. MX1, each with an average RA of 11 %. Among the bacteria, *Smithellaceae* sp. MA87 stands out as the most abundant member, with RA ranging between 3–10 %. This family was recently reclassified to the order Syntrophales [49] and proposed as propionate-degrading syntrophs [50]. The substrate preference was confirmed by the increased prevalence of *Smithellaceae* sp. MA87 in propionate-supplied reactor (M3), although MA87 was also abundant when lactate was the carbon source (M1). In butyrate-fed reactor (M2) *Syntrophomonadaceae* sp. MX35 and *Thermovirgaceae* sp. MA58 displayed a 3.9 fold-change increase in RA with respect to TP1, suggesting a possible role in butyric acid degradation, as already demonstrated for *Syntrophomonas* and *Syntrophaceticus* species [51].

The microbiome composition and organization were influenced by the different carbon sources supplied. The utilization of substrates, expressed as % reduction of COD, revealed that microbes exhibited higher efficiency in utilizing acetate and lactate compared to butyrate and propionate. This trend was particularly evident in media containing only one compound, where the specific substrate utilization exceeded 80 % (Table S3). On the other hand, the tested carbon sources had a minor impact on bioreactor performance than anticipated. In Experiment 2, the $CH_4$ production efficiency was comparable among lactate, butyrate and propionate, with values ranging between 2.2–2.5 $dm^3$/day (Table S3). Interestingly, specific methanogens increased in abundance under particular conditions (Fig. 1), with *Methanofollis liminatans* MB22 being abundant exclusively in reactor M1 and *Methanocorpusculum* sp. VB25 in M1 and M2. These archaea, along with *Methanoculleus* sp. MX1, are known hydrogenotrophs [52], implying the presence of syntrophic acetate-oxidizing bacteria (SAOB), given that no $H_2$ was supplied to the systems. Specifically, SAOB have the capacity to sustain the hydrogenotrophic methanogenesis via the reverse WL pathway, converting acetate into $H_2$ and $CO_2$, possibly in combination with the GSR pathway [12]. However, none of the investigated bacteria belonged to species previously reported as SAOB and a deeper exploration at the transcriptome level is necessary to confirm their presence. Specifically, the regulatory molecular mechanisms and the effect of dominant acidic products on $CH_4$ biogenesis have to be deciphered.

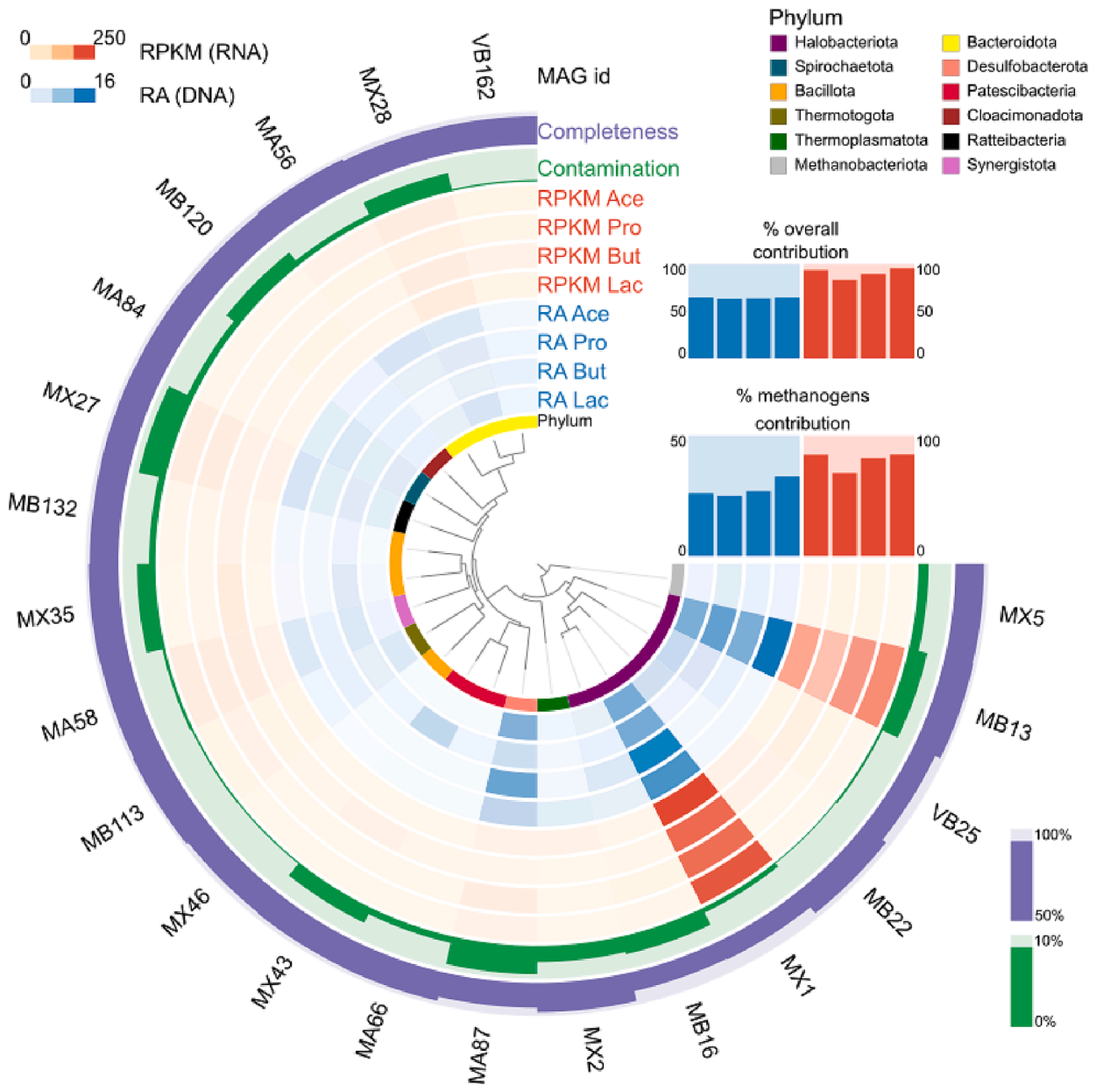


**Fig. 1.** Overview of the identified microbial taxa. Taxonomy at phylum level, completeness, contamination, average RA and average RPKM across the reactors, for the reconstructed MAGs. Only the taxa with RA of 1% or higher in at least one sample are reported. The collective contribution, as measured by RA and Reads Per Kilobase per Million mapped reads (RPKM), is drawn for the 26 selected MAGs (% overall contribution), and exclusively for the archaeal MAGs (% methanogens contribution), in comparison to the total of 178 reconstructed MAGs. Correspondence between MAG ID and full name can be found in Table S5.

### 3.2. Activity of methanogenic microcosms fed with different carboxylic acids

The investigation of the behavior of some key microbes was conducted through PCA on the top 500 highly expressed genes within the selected MAGs (Fig. S5). Notably, among the archaea, *M. soehngenii* MB13 and *Methanoculleus* sp. MX1 exhibited distinct transcriptional profiles between TP1 and TP2, underscoring a clear shift in activity upon the provision of pure substrates. Conversely, transcriptome levels in *M. liminatans* MB22 and *Methanocorpusculum* sp. VB25 demonstrated fluctuations dependent on the specific carbon sources under consideration. To validate the different contribution of acetotrophic and hydrogenotrophic pathways depending on the substrate provided, metatrascriptomic analyses of the microbiomes were performed. The changes in gene expression level between TP2 (day 884) and TP1 (day 751) are represented as $\log_2$FC calculated from three replicates (Materials and Methods).

#### 3.2.1. Hydrogenotrophic methanogenesis

The four HM exhibited substrate-dependent behaviors (Fig. 3), revealing distinct efficiency in establishing syntrophic relationships. *Methanoculleus* sp. MX1 was upregulating the final steps of the methanogenesis only when butyrate and propionate were provided as substrates. Specifically, the gene encoding the methyl-coenzyme M reductase (*mcr)* exhibited a $\log_2$FC of 2.55 and 1.69 in M2 and M3 reactors, respectively. The expression of *mcr* has been correlated with either $CH_4$ production rate or $CH_4$ yield, thereby confirming its status as a reliable and consistent [53]. Furthermore, the high hydrogenotrophic

activity in reactor M2 was substantiated by the statistically significant upregulation of *mtr* ($log_2FC = 1.62$) and *eha* ($log_2FC = 1.44$). The former encodes tetrahydro-methanopterin S-methyltransferase, which catalyzes the reaction before Mcr [54]. Conversely, the product of the latter gene fulfills an anaplerotic role within the energy-converting hydrogenase system. Eha activity ensures a continuous supply of reduced ferredoxin [55], which is subsequently utilized in the initial step of the hydrogenotrophic route for the conversion of $CO_2$ into formylmethanofuran by the formylmethanofuran dehydrogenase (*fwd/fmd*) [54], which is also upregulated. Transcriptomics results support previous isotopic findings [24], indicating that butyrate and propionate favored the hydrogenotrophic activity of *Methanoculleus* sp. MX1, despite comparable RA across different substrates (Fig. 1).

To delve deeper, in *Methanocorpusculum* sp. VB25 and *Methanofollis* liminatans MB22 the upregulation of methanogenesis was registered in multiple reactors, suggesting a high metabolic flexibility. In M1 reactor *Methanocorpusculum* sp. VB25 was likely flanking *Methanoculleus* sp. MX1 in $CH_4$ production, with the whole gene set having a $log_2FC > +1$, although only *mcr* was statistically significant (Fig. 3). Moreover, together with *M. liminatans* MB22, *Methanocorpusculum* sp. VB25 upregulated *mcr* in M4 reactor, with $log_2FC$ of 2.60 and 2.27 respectively ($p < 0.05$). Likely, these archaea sustained hydrogenotrophic methanogenesis amidst substrate competition with a putative SAOB [56], potentially *Smithellaceae* sp. MA87, particularly with the acetoclastic *M. soehngenii* MB13. As far as *M. liminatans* MB22, an increased activity was also found in M3 reactor (Fig. 3), with *mcr* being significantly upregulated ($log_2FC = 4.74$). Furthermore, significant upregulation was observed in the genes encoding methylenetetrahydromethanopterin dehydrogenase (*hmd/mtd*) and coenzyme F420 hydrogenase (*frh*), with $log_2FC$ of 5.28 and 1.79, respectively. Of particular interest is the overexpression of *frh*, which encodes a protein involved in the generation of $F_{420}H_2$ for the second and third reductive steps of methanogenesis [57], ensuring replenishment of necessary intermediates.

### 3.2.2. Acetoclastic methanogenesis

The transcriptome profile of *M. soehngenii* MB13 is strongly different in comparison to HM. First, acetate reduction was attributed to ACS activity and not the *ackA-pta* pathway, as previously demonstrated in *Methanothrix* species [58]. The expression level of *acs* did not show evidence of upregulation (Fig. 3). This outcome can be explained by the high availability of substrate in this condition (Table S4) and the measured FPK, remaining below 2500 in all samples (Table S8).

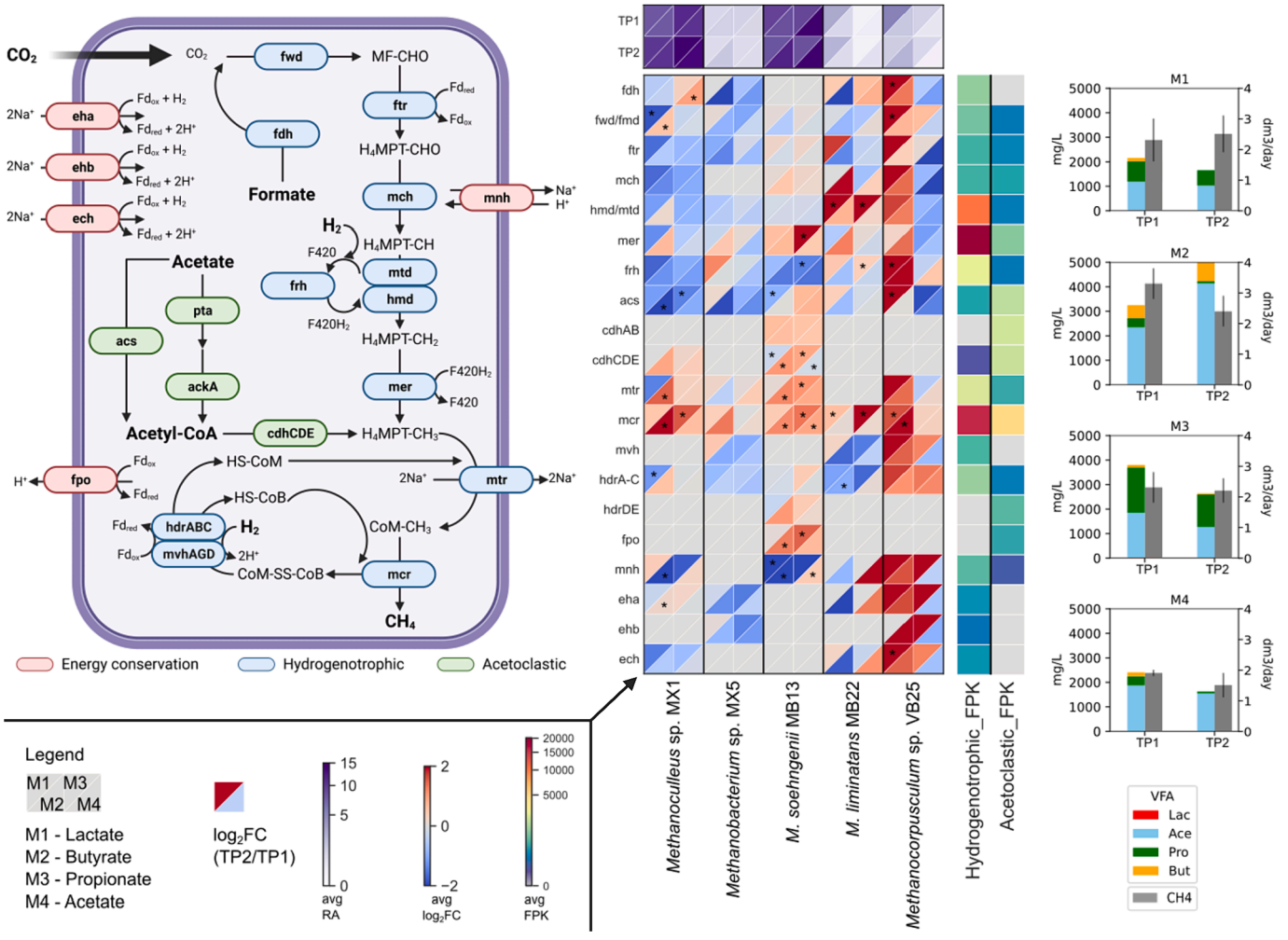


**Fig. 2.** Methanogenic activity of archaeal MAGs, differential expression under the prolonged reactor's activity and biochemical process indicator. The expression of genes related to methanogenesis, carbon assimilation, and energy conservation, along with the results of the differential expression analysis, are presented as $log_2FC$ values (Materials and Methods section). The $log_2FC$ of enzymes composed of multiple subunits is represented as the average value of all the detected subunits. Enzymes with at least one differentially expressed gene with p-value $< 0.05$ are marked with *. The RA of archaeal MAGs at the two time points is presented in the top panel. On the right side panel, the average FPK of genes involved in methanogenesis is reported for the acetoclastic and hydrogenotrophic populations. Genes not present and/or reconstructed in the analyzed MAGs were represented with the color gray. The barplot on the left side represents the methane production in $dm^3$/day and the VFA in mg/L for TP1 (day 751) and TP2 (day 884).

Nonetheless, acetoclastic methanogenesis remained active, as evidenced by a consistent methane yield [19] and by the *mcr* expression level ranging between 6500–8000 FPK at TP2 across all reactors. Additionally, genes encoding subunits *cdhCDE* of the carbon monoxide dehydrogenase/acetyl-CoA synthase (CODH/ACS) complex were upregulated and exhibited statistical significance (Fig. 3). This complex has a central role in the decomposition of Acetyl-CoA, oxidizing the carbonyl group to $CO_2$ and transferring the methyl group to tetrahydrosarcinapterin (THSPT) [59,60]. Another upregulated gene supporting the acetoclastic route was *fpo*, encoding the $F420H_2$ dehydrogenase. This membrane-bound enzyme is responsible for the reoxidation of coenzyme F420, which undergoes reduction during methanogenesis. Fpo activity is coupled with proton translocation across the cytoplasmic membrane, generating the proton motive force for ATP synthesis [61]. This behavior is likely the result of a high energy state reached by *M. soehngenii* MB13 thanks to the action of the FAD-dependent lactate dehydrogenase LDH (*glcD*). This enzyme degrades lactate into pyruvate, subsequently converted into acetate through pyruvate:ferredoxin oxidoreductase (*por*). The resulting acetate becomes available for acetoclastic methanogenesis, previously identified as the prevalent pathway in reactor M1 through stable isotope analysis [19]. These genes were reported to be active, with FPK values of 180 for *glcD* and 580 for *por* in reactor M1. This is the first time that such a mechanism has been evidenced in archaea, since previously it was found only in bacteria, including *A. woodii* [13] and *Moorella thermoacetica* [62]. Even though intriguing, the existence of this mechanism needs to be confirmed with a dedicated isolation and cultivation experiment.

Altogether, metatranscriptomics of archeal populations revealed a significantly high level of activity among acetoclastic and hydrogenotrophic members (Table S8), thus serving as validation for the $CH_4$ production rates reported (Fig. 2). Nevertheless, the extent of this activity is markedly contingent upon the ability to establish syntrophic relationships. In these interactions, various specialized microbes collaborate to collectively degrade the original substrate into acetate, which is subsequently converted by SAOB to fuel the hydrogenotrophic methanogenesis.

### 3.3. Multiple syntrophic metabolisms with carboxylic acids

The PCA conducted on the top highly expressed genes unveiled distinct behavioral patterns contingent upon the species under investigation (Fig. S5). Most bacteria exhibited a discernible dichotomy in transcriptional expression in response to the provision of mixed or pure carbon substrates. In contrast, species such as *Syntrophomonadaceae* sp. MX35 and *Smithellaceae* sp. MA87 showcased an expression profile more contingent on the type of carboxylic acid utilized, indicating a high degree of specificity in MAG metabolism. To decipher the trophic dependencies established between HM and the bacteria, the expression level of genes involved in lactate, butyrate, propionate and acetate degradation were investigated. Furthermore, the possible competition between acetoclastic archaea and homoacetogenic bacteria was also explored. Only bacteria with relevant expression level (average $>$ 5 RPKM in at least one reactor) were selected for this investigation (Table S5, Fig. S4).

#### 3.3.1. Versatile syntrophic fatty acid oxidation by uncultivated Mesotoga species

In reactor M1, lactate degradation is facilitated by the activity of *Mesotoga* sp. MB113 (Fig. 3), the sole MAG expressing *ldh* ($log_2FC$ = 1.25). The encoded lactate dehydrogenase converts lactate into pyruvate, a conversion made possible by the exergonic electron flow from reduced ferredoxin to $NAD^+$ [13]. This mechanism involves flavin-based electron bifurcation for energetic coupling, as previously demonstrated [63]. The expression of genes encoding the $H^+/Na^+$-translocating ferredoxin:$NAD^+$ oxidoreductase (*rnf*), the proton-translocating $NAD(P)^+$ transhydrogenase (*pntAB*) and NADH-quinone oxidoreductase (*nuo*), provides compelling evidence for the plausibility of this mechanism.

Moreover, *Mesotoga* sp. MB113 could also act as SAOB, through the expression of an alternative WL mediated by the GCS, as already proposed for other *Mesotoga* species [56]. More specifically, the glycine reductase complex (*grd*) and the GCS (*gcvPA*, *gcvPB*, *gcvH*) were expressed with $log_2FC > +1$ (Fig. 3). This result highlights the plasticity of this microbe, capable of exploiting various degradative pathways and establishing diverse syntrophic relationships. Specifically, it was feeding acetate to *M. soehngenii* MB13 or further converting it into $H_2$ and $CO_2$ to be utilized by HM.

#### 3.3.2. Predominant butyrate consumption by a Syntrophomonadaceae member

Among other bacteria, the transcriptomic profile of *Syntrophomonadaceae* sp. MX35 strongly indicates a significant commitment to butyrate oxidation. This putative role is further substantiated since all known butyrate oxidizers are classified into the family *Syntrophomonadaceae* [64]. They metabolize butyrate through beta-oxidation, encompassing an initial activation step, followed by a stepwise oxidation process from butyryl-CoA to two molecules of acetyl-CoA [65]. In reactor M2, *Syntrophomonadaceae* sp. MX35 upregulates numerous genes associated with this metabolic route (Fig. 3). Specifically, genes encoding the butyryl-CoA dehydrogenase (*bcd*) and two isoforms of enoyl-CoA hydratase (*paaF*, *crt*) were significantly overexpressed. These enzymes play a pivotal role in the oxidation of butyryl-CoA to crotonyl-CoA, followed by conversion into 3-hydroxybutanoyl-CoA. This intermediate undergoes further oxidation, initially yielding acetoacetyl-CoA through the action of 3-hydroxybutyryl-CoA dehydrogenase, ultimately culminating in the conversion to acetyl-CoA mediated by acetyl-CoA C-acetyltransferase. It is noteworthy that genes associated with these enzymatic reactions, namely *fadN*, *paaH* and *atoB* exhibited $log_2FC > +1$ and statistical significance (Fig. 3).

To facilitate this conversion, a membrane-level energy conservation mechanism is required [7]. *Syntrophomonadaceae* sp. MX35 exhibited upregulation of genes encoding the $H^+/Na^+$-translocating ferredoxin:$NAD^+$ oxidoreductase (*rnf*), also known as Rnf complex. This complex effectively couples the energy from $NAD^+$ reduction by ferredoxin to actively transport protons, generating a motive force across the cytoplasmic membrane [66]. These findings provide additional validation for the previously established mechanism, thus confirming the role of *Syntrophomonadaceae* sp. MX35 as a butyrate oxidizer.

The trained supervised ML algorithms provided further compelling evidence. The model detected 12 potential butyrate oxidizers within the 178 reconstructed MAGs: 8 members of *Syntrophomonadaceae*, 3 Syntrophales and a *Syntrophorhabdaceae* (Table S10). Notably, *Syntrophomonadaceae* sp. MX35 was among the predicted oxidizers, reinforcing its role in butyrate oxidation.

#### 3.3.3. Transcriptomic exploration unveils an intricate propionate degradation network

Propionate oxidation has been reported to occur through four alternative metabolic routes: (i) methylmalonyl-CoA, (ii) lactate, (iii) hydroxypropionyl and (iiii) dismutating pathways [67]. In *S. propionica,*

propionate conversion was demonstrated to take place via dismutation pathway [9]. Regrettably, due to a partial reconstruction of the *Smithellaceae* sp. MA87 (Table S5), only a limited number of genes associated with propionate oxidation were recovered. Nonetheless, metatranscriptomics revealed high transcriptional activity overall. Indeed, propionate activation was upregulated, with genes *gctA* and *gctB* showing a $log_2$FC of 1.08 and 1.24, respectively (Fig. 3). The encoded glutaconate-CoA transferase, homolog of propionate CoA-transferase, has already been shown to perform this function in *Ralstonia eutropha* [68]. Additionally, two isoforms of malate dehydrogenase exhibited upregulation, as genes *maeA* and *maeB* revealed a $log_2$FC of 1.27 in reactor M3. In addition to catalyzing the oxidative decarboxylation of (S)-malate, these two enzymes can also perform decarboxylation to convert oxaloacetate to pyruvate.

Among the other MAGs examined, only *Syntrophomonadaceae* sp. MX35 and *Mesotoga* sp. MB113 showed upregulated genes linked to the methylmalonyl-CoA pathway (Fig. 3). These include propionyl-CoA carboxylase (*ppcB*), methylmalonyl-CoA mutase (*mcmA2*), succinate dehydrogenase (*sdh*) and fumarate hydratase (*fum*). An intriguing possibility is the establishment of a syntrophic exchange where butyrate, produced via dismutation pathway by *Smithellaceae* sp. MA87, is taken up and metabolized by the butyrate-oxidizing *Syntrophomonadaceae* sp. MX35. The latter exhibited the overexpression of all beta-oxidation genes [65], starting from butyryl-CoA dehydrogenase (*bcd*) to acetyl-CoA C-acetyltransferase (*atoB*), demonstrating a high transcriptional activity (Fig. 3). This was further supported by upregulated energy conservation genes, including electron-confurcating hydrogenase (*hydABC*) and electron transfer flavoprotein (*etfAB*), with $log_2$FC of 4.54 and 2.23 in reactor M3, respectively. Specifically, ETF is accountable for oxidizing NADH while simultaneously reducing crotonyl-CoA and ferredoxin [69], whereas the HydABC complex facilitates reversible ferredoxin reduction by coupling it with the conversion of $H_2$ to $NAD^+$ reduction [63]. Although promising, this interaction still needs a more direct demonstration, as already reported for *Eubacteriaceae* species [70].

#### 3.3.4. Metabolic plasticity of putative SAOB: Balancing syntrophies and competitive dynamics

Further investigation of the syntrophic and competitive interactions for acetate revealed a high degree of complexity. Butyrate oxidizer *Syntrophomonadaceae* sp. MX35 upregulated genes associated with acetate metabolism in M2 and M3 reactors (Fig. 3). There, it likely competed with *M. soehngenii* MB13 and formed syntrophic partnerships with HM. Following butyrate or propionate oxidation, acetate is metabolized into formate through the reverse WL pathway [71]. Genes encoding acetate kinase (*ackA*) and phosphate acetyltransferase (*pta*), responsible for converting acetate into acetyl-CoA, were notably overexpressed. Furthermore, subsequent steps of the canonical pathway were also upregulated, showing a significant expression increase in *metF*, *folD* and *fhs* genes (Fig. 3). These genes correspond to methylenetetrahydrofolate reductase (MTHFR) and dehydrogenase (FolD), and formate-tetrahydrofolate ligase (FTHFS), which collectively enable the conversion of intermediate compounds into formate [71]. Although methanogenesis from formate has been previously demonstrated [72], the observed upregulation of genes encoding formate dehydrogenase (*fdh*) implies an additional conversion into $H_2$ and $CO_2$. This ultimately provides a continuous source of substrate for HM, reflecting the high activity registered for *Methanocorpusculum* sp. VB25 and *M. liminatans* MB22 in reactors M2 and M3 (Fig. 2).

Transcriptional changes observed highlighted how acetoclastic *M. soehngenii* MB13 always engaged competition with the bacterial counterpart, since genes involved in the conventional and alternative WL pathways were found to be upregulated and RA of SAOB increased (Fig. 3). A similar competitive event has already been documented in biowaste digester, where syntrophic acetate oxidation replaced acetoclastic methanogenesis [73]. The HM were sustained in their biomethanation activity through $H_2$ and $CO_2$ generated by the degradative activity of syntrophic species, including *Mesotoga* sp. MB113, *Syntrophomonadaceae* sp. MX35 and *Smithellaceae* sp. MA87, particularly in butyrate- and propionate-fed reactors. Conversely, in reactor M4, *M. soehngenii* MB13 prevailed in the competition for substrate, exhibiting high transcriptional activity for acetoclastic methanogenesis genes (Table S8). The downregulation of the hydrogenotrophic pathway in other archaeal species, indicating limited availability of $H_2$ and $CO_2$, further supports *M. soehngenii* MB13 as the primary acetate consumer (Fig. 3).

Moreover, proposed syntrophies include potential butyrate uptake by *Syntrophomonadaceae* sp. MX35, possibly originating from pyruvate degradation catalyzed by *Smithellaceae* sp. MA87. Subsequently, *Syntrophomonadaceae* sp. MX35 could convert the butyrate through the alternative WL pathway, and this is supported by the observed upregulation of genes encoding formate dehydrogenase (*fdh, fdhAB*) with $log_2$FC of 4.12 and 4.65, respectively (Fig. 3). To bolster and provide a more comprehensive understanding of these findings, FBA stands as a valid alternative, having the potential to elucidate the actual flow of metabolites and predict the potential distribution of resources within a microbiome.

### 3.4. Integrating flux-balance analysis to describe the metabolic relationship between microbes

GEMs were reconstructed for all the MAGs with an abundance exceeding 1 % in at least one sample, resulting in a comprehensive community-specific model comprising 24,907 reactions (±498) and 22,825 metabolites (±458). To better define the reaction bounds and improve the metabolic models predictivity, transcriptomic data were incorporated. The accuracy of micom-simulated outcomes was validated against the growth rate calculated by *Coprothermobacter*, as previously described [48]. The correlation between the model-predicted growth rates and corresponding species replication rates yielded a positive correlation coefficient of 0.44 (p-value $< 2^{e-5}$).

Biochemical data, including VFA and $CH_4$ production (Table S4, S11), were employed as additional constraints. Within reactor M1, the predominant contributors to lactate consumption were *Mesotoga* MB113 and Bacillota sp. MB132. Indeed, metabolic prediction confirmed the capacity of these bacteria to consume lactate, yielding essential substrates such as $CO_2$ and $H_2$, crucial for HM. Specifically, *Mesotoga* MB113 was predicted as L-Serine producer, with *Methanoculleus* sp. MX1 identified as the primary consumer. This observation underscores the concept that, in syntrophic interactions, not only are $CO_2$ and $H_2$ shared, but also other compounds, including amino acids, as previously proposed in $CO_2$ fixating microbiomes [74].

Within reactor M2, simulations showed a small butyrate accumulation in the medium, as observed in the biochemical results (Table S4). The primary consumers were identified as Paceibacterales sp. MX43 and *Syntrophomonadaceae* sp. MX35. The carbon fluxes predicted for conversion of butyrate into acetate corroborated the role proposed by their transcriptomic profile (Fig. 3). Concurrently, *Thermovirgaceae* sp. MA58 was identified as homoacetogen, as already documented in reactors supplied with acetate and butyrate [19]. FBA further revealed the conversion of propionate to $CO_2$ and $H_2$ by *Rectinemataceae* sp. MA84 and, similarly to *Mesotoga* MB113, it was proposed as L-Glutamate and L-Serine producer, two compounds predominantly consumed by *Methanoculleus* sp. MX1. As observed above, acetate can be used by *Methanoculleus* sp. MX1 but not for $CH_4$ production. Carbon fluxes showed that it can be converted to various amino acids, with a notable emphasis on L-aspartate and glycine.

Lastly, the preeminent acetate-oxidizer across all samples was identified as *Smithellaceae* sp. MA87, exhibiting the peak acetate flux in TP2 of M4 reactor. In *M. soehngenii* MB13, metabolic prediction revealed increased acetate consumption, competing with SAOB. Simulations suggested a shared niche for substrate, exchanging compounds for

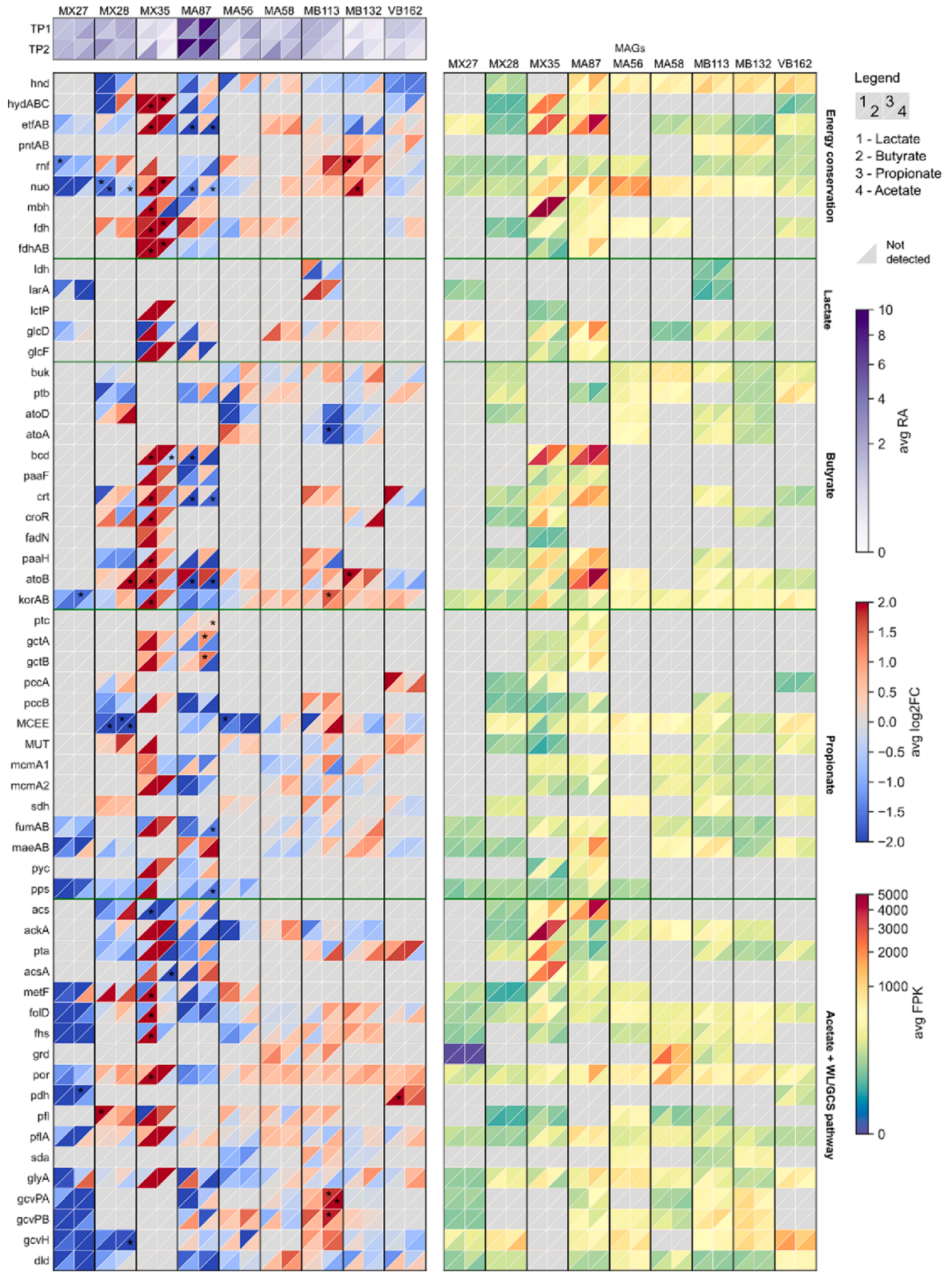


**Fig. 3.** Activity of bacterial MAGs and differential expression under the prolonged reactor's activity with each substrate. The expression of genes related to energy conservation, lactate, butyrate, propionate and acetate metabolism along with the results of the differential expression analysis, are presented as $\log_2$FC values (Materials and Methods section). The $\log_2$FC of enzymes composed of multiple subunits is represented as the average value of all the detected subunits. Enzymes with at least one differentially expressed gene with p-value $< 0.05$ are marked with *. The RA of bacterial MAGs at the two time points is presented in the top panel. On the right side panel, the average FPK of syntrophic metabolism genes is reported for the bacterial populations. Genes not present and/or reconstructed in the analyzed MAGs were represented with the color gray. Correspondence between MAG ID and full name can be found in Table S5.

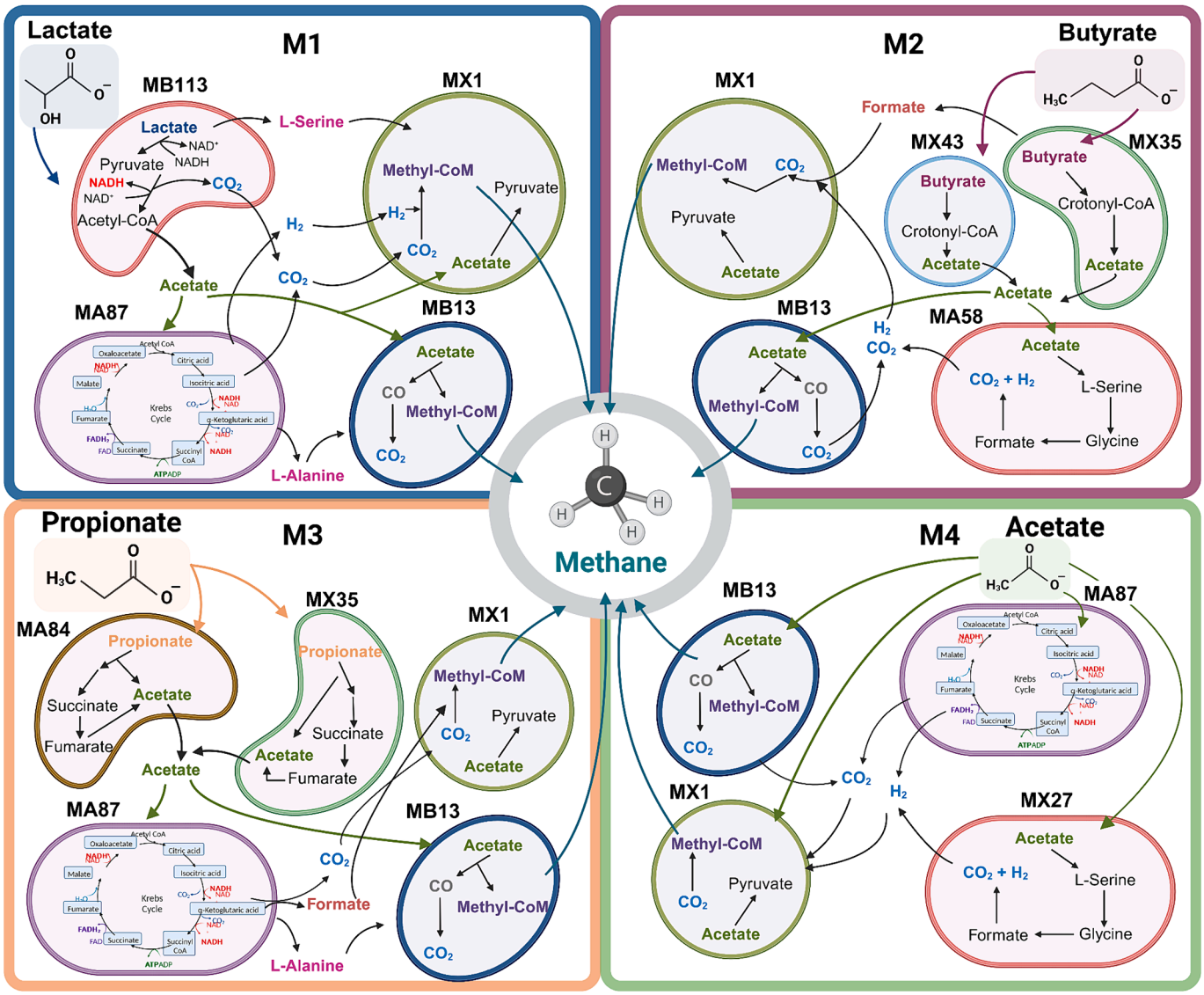


**Fig. 4.** Schematic representation illustrates the principal metabolic fluxes between the predominant species in each reactor, offering a comprehensive visualization of the intricate network of interactions within the microbiome. The central production of each reactor is represented by $CH_4$, which was produced by the acetoclastic MB13 and hydrogenotrophic MX1 archaea. Correspondence between MAG ID and full name can be found in Table S5.

mutual benefit. The main interaction could be from *Smithellaceae* MA87 secreting L-Alanine and the archaeon consuming it. Metabolic reconstruction allowed to clarify the mechanisms behind carboxylic acid degradation in complex anaerobic microbiomes (Fig. 4), supporting the inferences derived from transcriptome analysis, as proposed in recent metatranscriptomics studies [25].

## 4. Conclusion

The use of a multi-omics approach to characterize complex microbiomes allowed to pinpoint the key microbes involved in the AD process, to associate them with specific metabolic roles and unravel underlying syntrophic interactions. Transcriptomics responses validated previous hypotheses, wherein dominant carbon source is the main driver for the pathways of methanogenesis. Specifically, acetate and lactate favored the acetotrophic route, while the hydrogenotrophic methanogenesis was preferred in butyrate and propionate enriched feedstocks. Additionally, the acetoclastic *M. soehngenii* showed an undocumented ability in processing the lactate for growth, through the expression of a FAD-dependent lactate dehydrogenase. Three putative syntrophs emerged from metatranscriptomic and data-driven ML classification, namely *Mesotoga*, *Syntrophomonadaceae*, and *Smithellaceae*, identified as the main responsible for the degradation of lactate, butyrate and acetate, respectively. Transcriptomics revealed shared features among carboxylic acid-oxidizing bacteria, including beta-oxidation or methylmalonyl-CoA pathways, multiple formate dehydrogenases, and electron bifurcation/confurcation systems. Integrating multi-omics layers into GEMs confirmed the syntrophic roles previously proposed and unveiled additional, less common yet significant, dynamics. Despite the effectiveness of genome-centric metatranscriptomics and FBA in investigating the behavior of individual members within complex microbiomes, limitations persist. Future enhancements in sequencing technologies, including single-cell resolution, are anticipated to expand our capabilities to unravel this complexity. This advancement will enable the exploration of a broader spectrum of developmental and metabolic gene expression programs, representing a significant stride in deciphering the yet unknown microbial dark matter.

## CRediT authorship contribution statement

**Gabriele Ghiotto:** Writing – review & editing, Writing – original draft, Visualization, Software, Methodology, Formal analysis, Data curation. **Anna Detman-Ignatowska:** Writing – review & editing, Methodology, Investigation, Data curation, Conceptualization. **Aleksandra Chojnacka:** Methodology, Investigation, Data curation. **Esteban Orellana:** Writing – original draft, Visualization, Software, Methodology, Investigation, Data curation. **Nicola de Bernardini:** Software, Methodology, Investigation, Data curation. **Sofia Fraulini:** Writing – original draft, Software, Methodology, Investigation. **Laura Treu:** Writing – review & editing, Supervision, Resources, Funding acquisition. **Anna Sikora:** Writing – review & editing, Methodology, Investigation, Data curation, Conceptualization. **Stefano Campanaro:** Writing – review & editing, Writing – original draft, Supervision, Resources, Funding acquisition.

## Declaration of competing interest

The authors declare that they have no known competing financial interests or personal relationships that could have appeared to influence the work reported in this paper.

## Data availability

Raw data from metagenomic and metatranscriptomic analyses generated in this study have been deposited in the NCBI under BioProject number PRJNA972863. Data will be made available on request.

## Acknowledgements

We acknowledge the support of The National Science Centre, Poland, through the UMO-2015/17/B/NZ9/01718 grant awarded for the years 2016-2019. This work was financially supported by the project LIFE20 CCM/GR/001642 – LIFE CO2toCH4 of the European Union LIFE + program. Anna Detman-Ignatowska was supported by the Foundation for Polish Science (FNP). Esteban Orellana was supported by the EMBO Postdoctoral fellowship (ALT 739-2022). We would like to thank Jan Gawor and Robert Gromadka for RNA sequencing support.

## Appendix A. Supplementary data

Supplementary data to this article can be found online at https://doi.org/10.1016/j.cej.2024.151390.

## References

[1] T. Kunatsa, X. Xia, A review on anaerobic digestion with focus on the role of biomass co-digestion, modelling and optimisation on biogas production and enhancement, Bioresour. Technol. 344 (2022) 126311, https://doi.org/10.1016/j.biortech.2021.126311.

[2] P.G. Kougias, I. Angelidaki, Biogas and its opportunities—A review, Front. Environ. Sci. Eng. 12 (2018) 14, https://doi.org/10.1007/s11783-018-1037-8.

[3] V.B. Centurion, A. Rossi, E. Orellana, G. Ghiotto, B. Kakuk, M.S. Morlino, A. Basile, G. Zampieri, L. Treu, S. Campanaro, A unified compendium of prokaryotic and viral genomes from over 300 anaerobic digestion microbiomes, Environ. Microbiome 19 (2024) 1, https://doi.org/10.1186/s40793-023-00545-2.

[4] P. Worm, J.J. Koehorst, M. Visser, V.T. Sedano-Núñez, P.J. Schaap, C.M. Plugge, D. Z. Sousa, A.J.M. Stams, A genomic view on syntrophic versus non-syntrophic lifestyle in anaerobic fatty acid degrading communities, Biochim. Biophys. Acta BBA - Bioenerg. 2014 (1837) 2004–2016, https://doi.org/10.1016/j.bbabio.2014.06.005.

[5] J.R. Sieber, M.J. McInerney, R.P. Gunsalus, Genomic insights into syntrophy: the paradigm for anaerobic metabolic cooperation, Annu. Rev. Microbiol. 66 (2012) 429–452, https://doi.org/10.1146/annurev-micro-090110-102844.

[6] N. Müller, D. Schleheck, B. Schink, Involvement of NADH:acceptor oxidoreductase and butyryl coenzyme A dehydrogenase in reversed electron transport during syntrophic butyrate oxidation by Syntrophomonas wolfei, J. Bacteriol. 191 (2009) 6167–6177, https://doi.org/10.1128/JB.01605-08.

[7] M.J. McInerney, L. Rohlin, H. Mouttaki, U. Kim, R.S. Krupp, L. Rios-Hernandez, J. Sieber, C.G. Struchtemeyer, A. Bhattacharyya, J.W. Campbell, R.P. Gunsalus, The genome of Syntrophus aciditrophicus: Life at the thermodynamic limit of microbial growth, Proc. Natl. Acad. Sci. 104 (2007) 7600–7605, https://doi.org/10.1073/pnas.0610456104.

[8] M. Westerholm, M. Calusinska, J. Dolfing, Syntrophic propionate-oxidizing bacteria in methanogenic systems, FEMS Microbiol. Rev. 46 (2022) fuab057, https://doi.org/10.1093/femsre/fuab057.

[9] F.A.M. de Bok, A.J.M. Stams, C. Dijkema, D.R. Boone, Pathway of propionate oxidation by a syntrophic culture of Smithella propionica and Methanospirillum hungatei, Appl. Environ. Microbiol. 67 (2001) 1800–1804, https://doi.org/10.1128/AEM.67.4.1800-1804.2001.

[10] M. Westerholm, S. Roos, A. Schnürer, Syntrophaceticus schinkii gen. nov., sp. nov., an anaerobic, syntrophic acetate-oxidizing bacterium isolated from a mesophilic anaerobic filter, FEMS Microbiol. Lett. 309 (2010) 100–104, https://doi.org/10.1111/j.1574-6968.2010.02023.x.

[11] K. Schuchmann, V. Müller, Energetics and application of heterotrophy in acetogenic bacteria, Appl. Environ. Microbiol. 82 (2016) 4056–4069, https://doi.org/10.1128/AEM.00882-16.

[12] Y. Song, J.S. Lee, J. Shin, G.M. Lee, S. Jin, S. Kang, J.-K. Lee, D.R. Kim, E.Y. Lee, S. C. Kim, S. Cho, D. Kim, B.-K. Cho, Functional cooperation of the glycine synthase-reductase and Wood-Ljungdahl pathways for autotrophic growth of Clostridium drakei, Proc. Natl. Acad. Sci. 117 (2020) 7516–7523, https://doi.org/10.1073/pnas.1912289117.

[13] M.C. Weghoff, J. Bertsch, V. Müller, A novel mode of lactate metabolism in strictly anaerobic bacteria, Environ. Microbiol. 17 (2015) 670–677, https://doi.org/10.1111/1462-2920.12493.

[14] L. Westphal, A. Wiechmann, J. Baker, N.P. Minton, V. Müller, The Rnf complex is an energy-coupled transhydrogenase essential to reversibly link cellular NADH and ferredoxin pools in the acetogen Acetobacterium woodii, J. Bacteriol. 200 (2018), https://doi.org/10.1128/jb.00357-18.

[15] X. Zhu, S. Campanaro, L. Treu, R. Seshadri, N. Ivanova, P.G. Kougias, N. Kyrpides, I. Angelidaki, Metabolic dependencies govern microbial syntrophies during methanogenesis in an anaerobic digestion ecosystem, Microbiome 8 (2020) 22, https://doi.org/10.1186/s40168-019-0780-9.

[16] S. Ishii, S. Suzuki, T.M. Norden-Krichmar, A. Tenney, P.S.G. Chain, M.B. Scholz, K. H. Nealson, O. Bretschger, A novel metatranscriptomic approach to identify gene expression dynamics during extracellular electron transfer, Nat. Commun. 4 (2013) 1601, https://doi.org/10.1038/ncomms2615.

[17] L. Treu, S. Campanaro, P.G. Kougias, X. Zhu, I. Angelidaki, Untangling the effect of fatty acid addition at species level revealed different transcriptional responses of the biogas microbial community members, Environ. Sci. Technol. 50 (2016) 6079–6090, https://doi.org/10.1021/acs.est.6b00296.

[18] Y. Jia, S.-K. Ng, H. Lu, M. Cai, P.K.H. Lee, Genome-centric metatranscriptomes and ecological roles of the active microbial populations during cellulosic biomass anaerobic digestion, Biotechnol. Biofuels 11 (2018) 117, https://doi.org/10.1186/s13068-018-1121-0.

[19] A. Detman, M. Bucha, L. Treu, A. Chojnacka, Ł. Pleśniak, A. Salamon, E. Łupikasza, R. Gromadka, J. Gawor, A. Gromadka, W. Drzewicki, M. Jakubiak, M. Janiga, I. Matyasik, M.K. Błaszczyk, M.O. Jędrysek, S. Campanaro, A. Sikora, Evaluation of acidogenesis products' effect on biogas production performed with metagenomics and isotopic approaches, Biotechnol. Biofuels 14 (2021) 125, https://doi.org/10.1186/s13068-021-01968-0.

[20] A. Basile, G. Zampieri, A. Kovalovszki, B. Karkaria, L. Treu, K.R. Patil, S. Campanaro, Modelling of microbial interactions in anaerobic digestion: from black to glass box, Curr. Opin. Microbiol. 75 (2023) 102363, https://doi.org/10.1016/j.mib.2023.102363.

[21] M. Kumar, B. Ji, K. Zengler, J. Nielsen, Modelling approaches for studying the microbiome, Nat. Microbiol. 4 (2019) 1253–1267, https://doi.org/10.1038/s41564-019-0491-9.

[22] X. Fang, C.J. Lloyd, B.O. Palsson, Reconstructing organisms in silico: genome-scale models and their emerging applications, Nat. Rev. Microbiol. 18 (2020) 731–743, https://doi.org/10.1038/s41579-020-00440-4.

[23] A. Weimann, K. Mooren, J. Frank, P.B. Pope, A. Bremges, A.C. McHardy, From genomes to phenotypes: Traitar, the microbial trait analyzer, Bioinformatics (2016), https://doi.org/10.1101/043315.

[24] F. Farrell, O.S. Soyer, C. Quince, Machine learning based prediction of functional capabilities in metagenomically assembled microbial genomes, (2018) 307157. https://doi.org/10.1101/307157.

[25] A. Singh, A. Schnürer, J. Dolfing, M. Westerholm, Syntrophic entanglements for propionate and acetate oxidation under thermophilic and high-ammonia conditions, ISME J. (2023) 1–13, https://doi.org/10.1038/s41396-023-01504-y.

[26] G. Ghiotto, N. De Bernardini, G. Giangeri, P. Tsapekos, M. Gaspari, P.G. Kougias, S. Campanaro, I. Angelidaki, L. Treu, From microbial heterogeneity to evolutionary insights: A strain-resolved metagenomic study of H2S-induced changes in

anaerobic biofilms, Chem. Eng. J. 485 (2024) 149824, https://doi.org/10.1016/j.cej.2024.149824.
[27] A.M. Bolger, M. Lohse, B. Usadel, Trimmomatic: a flexible trimmer for Illumina sequence data, Bioinformatics 30 (2014) 2114–2120, https://doi.org/10.1093/bioinformatics/btu170.
[28] B. Bushnell, J. Rood, E. Singer, BBMerge – Accurate paired shotgun read merging via overlap, PLOS ONE 12 (2017) e0185056.
[29] D. Li, C.-M. Liu, R. Luo, K. Sadakane, T.-W. Lam, MEGAHIT: an ultra-fast single-node solution for large and complex metagenomics assembly via succinct de Bruijn graph, Bioinformatics 31 (2015) 1674–1676, https://doi.org/10.1093/bioinformatics/btv033.
[30] Y.-W. Wu, B.A. Simmons, S.W. Singer, MaxBin 2.0: an automated binning algorithm to recover genomes from multiple metagenomic datasets, Bioinformatics 32 (2016) 605–607, https://doi.org/10.1093/bioinformatics/btv638.
[31] D.D. Kang, J. Froula, R. Egan, Z. Wang, MetaBAT, an efficient tool for accurately reconstructing single genomes from complex microbial communities, PeerJ 3 (2015) e1165.
[32] D.D. Kang, F. Li, E. Kirton, A. Thomas, R. Egan, H. An, Z. Wang, MetaBAT 2: an adaptive binning algorithm for robust and efficient genome reconstruction from metagenome assemblies, PeerJ 7 (2019) e7359.
[33] J.N. Nissen, J. Johansen, R.L. Allesøe, C.K. Sønderby, J.J.A. Armenteros, C. H. Grønbech, L.J. Jensen, H.B. Nielsen, T.N. Petersen, O. Winther, S. Rasmussen, Improved metagenome binning and assembly using deep variational autoencoders, Nat. Biotechnol. 39 (2021) 555–560, https://doi.org/10.1038/s41587-020-00777-4.
[34] M.R. Olm, C.T. Brown, B. Brooks, J.F. Banfield, dRep: a tool for fast and accurate genomic comparisons that enables improved genome recovery from metagenomes through de-replication, ISME J. 11 (2017) 2864–2868, https://doi.org/10.1038/ismej.2017.126.
[35] R.M. Bowers, N.C. Kyrpides, R. Stepanauskas, M. Harmon-Smith, D. Doud, T.B. K. Reddy, F. Schulz, J. Jarett, A.R. Rivers, E.A. Eloe-Fadrosh, S.G. Tringe, N. N. Ivanova, A. Copeland, A. Clum, E.D. Becraft, R.R. Malmstrom, B. Birren, M. Podar, P. Bork, G.M. Weinstock, G.M. Garrity, J.A. Dodsworth, S. Yooseph, G. Sutton, F.O. Glöckner, J.A. Gilbert, W.C. Nelson, S.J. Hallam, S.P. Jungbluth, T. J.G. Ettema, S. Tighe, K.T. Konstantinidis, W.-T. Liu, B.J. Baker, T. Rattei, J. A. Eisen, B. Hedlund, K.D. McMahon, N. Fierer, R. Knight, R. Finn, G. Cochrane, I. Karsch-Mizrachi, G.W. Tyson, C. Rinke, A. Lapidus, F. Meyer, P. Yilmaz, D. H. Parks, A. Murat Eren, L. Schriml, J.F. Banfield, P. Hugenholtz, T. Woyke, Minimum information about a single amplified genome (MISAG) and a metagenome-assembled genome (MIMAG) of bacteria and archaea, Nat. Biotechnol. 35 (2017) 725–731, https://doi.org/10.1038/nbt.3893.
[36] A. Chklovski, D.H. Parks, B.J. Woodcroft, G.W. Tyson, CheckM2: a rapid, scalable and accurate tool for assessing microbial genome quality using machine learning, Nat. Methods 20 (2023) 1203–1212, https://doi.org/10.1038/s41592-023-01940-w.
[37] B.J. Woodcroft, CoverM, (2023). https://github.com/wwood/CoverM (accessed March 30, 2023).
[38] P.-A. Chaumeil, A.J. Mussig, P. Hugenholtz, D.H. Parks, GTDB-Tk v2: memory friendly classification with the genome taxonomy database, Bioinformatics 38 (2022) 5315–5316, https://doi.org/10.1093/bioinformatics/btac672.
[39] F. Asnicar, A.M. Thomas, F. Beghini, C. Mengoni, S. Manara, P. Manghi, Q. Zhu, M. Bolzan, F. Cumbo, U. May, J.G. Sanders, M. Zolfo, E. Kopylova, E. Pasolli, R. Knight, S. Mirarab, C. Huttenhower, N. Segata, Precise phylogenetic analysis of microbial isolates and genomes from metagenomes using PhyloPhlAn 3.0, Nat. Commun. 11 (2020) 2500, https://doi.org/10.1038/s41467-020-16366-7.
[40] D. Hyatt, G.-L. Chen, P.F. LoCascio, M.L. Land, F.W. Larimer, L.J. Hauser, Prodigal: prokaryotic gene recognition and translation initiation site identification, BMC Bioinformatics 11 (2010) 119, https://doi.org/10.1186/1471-2105-11-119.
[41] C.P. Cantalapiedra, A. Hernández-Plaza, I. Letunic, P. Bork, J. Huerta-Cepas, eggNOG-mapper v2: functional annotation, orthology assignments, and domain prediction at the metagenomic scale, Mol. Biol. Evol. 38 (2021) 5825–5829, https://doi.org/10.1093/molbev/msab293.
[42] M. Kanehisa, M. Furumichi, Y. Sato, M. Kawashima, M. Ishiguro-Watanabe, KEGG for taxonomy-based analysis of pathways and genomes, Nucleic Acids Res. 51 (2023) D587–D592, https://doi.org/10.1093/nar/gkac963.
[43] B. Langmead, S.L. Salzberg, Fast gapped-read alignment with Bowtie 2, Nat. Methods 9 (2012) 357–359, https://doi.org/10.1038/nmeth.1923.
[44] G.H. Putri, S. Anders, P.T. Pyl, J.E. Pimanda, F. Zanini, Analysing high-throughput sequencing data in Python with HTSeq 2.0, Bioinformatics 38 (2022) 2943–2945, https://doi.org/10.1093/bioinformatics/btac166.
[45] M.I. Love, W. Huber, S. Anders, Moderated estimation of fold change and dispersion for RNA-seq data with DESeq2, Genome Biol. 15 (2014) 550, https://doi.org/10.1186/s13059-014-0550-8.
[46] J. Zimmermann, C. Kaleta, S. Waschina, gapseq: informed prediction of bacterial metabolic pathways and reconstruction of accurate metabolic models, Genome Biol. 22 (2021) 81, https://doi.org/10.1186/s13059-021-02295-1.
[47] C. Diener, S.M. Gibbons, O. Resendis-Antonio, MICOM: Metagenome-Scale Modeling To Infer Metabolic Interactions in the Gut Microbiota, mSystems 5 (2020) 10.1128/msystems.00606-19. https://doi.org/10.1128/msystems.00606-19.
[48] G. Zampieri, S. Campanaro, C. Angione, L. Treu, Metatranscriptomics-guided genome-scale metabolic modeling of microbial communities, Cell Rep. Methods 3 (2023) 100383, https://doi.org/10.1016/j.crmeth.2022.100383.
[49] D.W. Waite, M. Chuvochina, C. Pelikan, D.H. Parks, P. Yilmaz, M. Wagner, A. Loy, T. Naganuma, R. Nakai, W.B. Whitman, M.W. Hahn, J. Kuever, P. Hugenholtz, Proposal to reclassify the proteobacterial classes Deltaproteobacteria and Oligoflexia, and the phylum Thermodesulfobacteria into four phyla reflecting major functional capabilities, Int. J. Syst. Evol. Microbiol. 70 (2020) 5972–6016, https://doi.org/10.1099/ijsem.0.004213.
[50] Y. Liu, D.L. Balkwill, H.C. Aldrich, G.R. Drake, D.R. Boone, Characterization of the anaerobic propionate-degrading syntrophs Smithella propionica gen. nov., sp. nov. and Syntrophobacter wolinii, Int. J. Syst. Evol. Microbiol. 49 (1999) 545–556, https://doi.org/10.1099/00207713-49-2-545.
[51] A.A. Nikitina, A.Y. Kallistova, D.S. Grouzdev, T.V. Kolganova, A.A. Kovalev, D. A. Kovalev, V. Panchenko, I. Zekker, A.N. Nozhevnikova, Y.V. Litti, Syntrophic butyrate-oxidizing consortium mitigates acetate inhibition through a shift from acetoclastic to hydrogenotrophic methanogenesis and alleviates VFA stress in thermophilic anaerobic digestion, Appl. Sci. 13 (2023) 173, https://doi.org/10.3390/app13010173.
[52] F.B. Sarmiento, J.A. Leigh, W.B. Whitman, Chapter three - Genetic Systems for Hydrogenotrophic Methanogens, in: A.C. Rosenzweig, S.W. Ragsdale (Eds.), Methods Enzymol, Academic Press, 2011, pp. 43–73, 10.1016/B978-0-12-385112-3.00003-2.
[53] D. Yu, J. Zhang, B. Chulu, M. Yang, I. Nopens, Y. Wei, Ammonia stress decreased biomarker genes of acetoclastic methanogenesis and second peak of production rates during anaerobic digestion of swine manure, Bioresour. Technol. 317 (2020) 124012, https://doi.org/10.1016/j.biortech.2020.124012.
[54] P.N. Evans, J.A. Boyd, A.O. Leu, B.J. Woodcroft, D.H. Parks, P. Hugenholtz, G. W. Tyson, An evolving view of methane metabolism in the Archaea, Nat. Rev. Microbiol. 17 (2019) 219–232, https://doi.org/10.1038/s41579-018-0136-7.
[55] T.J. Lie, K.C. Costa, B. Lupa, S. Korpole, W.B. Whitman, J.A. Leigh, Essential anaplerotic role for the energy-converting hydrogenase Eha in hydrogenotrophic methanogenesis, Proc. Natl. Acad. Sci. 109 (2012) 15473–15478, https://doi.org/10.1073/pnas.1208779109.
[56] M.K. Nobu, T. Narihiro, C. Rinke, Y. Kamagata, S.G. Tringe, T. Woyke, W.-T. Liu, Microbial dark matter ecogenomics reveals complex synergistic networks in a methanogenic bioreactor, ISME J. 9 (2015) 1710–1722, https://doi.org/10.1038/ismej.2014.256.
[57] E.L. Hendrickson, J.A. Leigh, Roles of coenzyme F420-reducing hydrogenases and hydrogen- and F420-dependent methylenetetrahydromethanopterin dehydrogenases in reduction of F420 and production of hydrogen during methanogenesis, J. Bacteriol. 190 (2008) 4818–4821, https://doi.org/10.1128/jb.00255-08.
[58] M.C. Gagliano, P. Sampara, C.M. Plugge, H. Temmink, D. Sudmalis, R.M. Ziels, Functional insights of salinity stress-related pathways in metagenome-resolved methanothrix genomes, Appl. Environ. Microbiol. 88 (2022) e0244921.
[59] J.A. Maupin-Furlow, J.G. Ferry, Analysis of the CO dehydrogenase/acetyl-coenzyme A synthase operon of Methanosarcina thermophila, J. Bacteriol. 178 (1996) 6849–6856, https://doi.org/10.1128/jb.178.23.6849-6856.1996.
[60] D.A. Grahame, Catalysis of acetyl-CoA cleavage and tetrahydrosarcinapterin methylation by a carbon monoxide dehydrogenase-corrinoid enzyme complex, J. Biol. Chem. 266 (1991) 22227–22233, https://doi.org/10.1016/S0021-9258(18)54558-0.
[61] S. Bäumer, T. Ide, C. Jacobi, A. Johann, G. Gottschalk, U. Deppenmeier, The F420H2 dehydrogenase from Methanosarcina mazei is a redox-driven proton pump closely related to NADH dehydrogenases*, J. Biol. Chem. 275 (2000) 17968–17973, https://doi.org/10.1074/jbc.M000650200.
[62] F.P. Rosenbaum, A. Poehlein, R. Egelkamp, R. Daniel, S. Harder, H. Schlüter, M. C. Schoelmerich, Lactate metabolism in strictly anaerobic microorganisms with a soluble NAD+-dependent l-lactate dehydrogenase, Environ. Microbiol. 23 (2021) 4661–4672, https://doi.org/10.1111/1462-2920.15657.
[63] W. Buckel, R.K. Thauer, Energy conservation via electron bifurcating ferredoxin reduction and proton/Na+ translocating ferredoxin oxidation, Biochim. Biophys. Acta BBA - Bioenerg. 2013 (1827) 94–113, https://doi.org/10.1016/j.bbabio.2012.07.002.
[64] M.J. McInerney, C.G. Struchtemeyer, J. Sieber, H. Mouttaki, A.J.M. Stams, B. Schink, L. Rohlin, R.P. Gunsalus, Physiology, ecology, phylogeny, and genomics of microorganisms capable of syntrophic metabolism, Ann. n. y. Acad. Sci. 1125 (2008) 58–72, https://doi.org/10.1196/annals.1419.005.
[65] N. Müller, P. Worm, B. Schink, A.J.M. Stams, C.M. Plugge, Syntrophic butyrate and propionate oxidation processes: from genomes to reaction mechanisms, Environ. Microbiol. Rep. 2 (2010) 489–499, https://doi.org/10.1111/j.1758-2229.2010.00147.x.
[66] L. Wang, P. Bradstock, C. Li, M.J. McInerney, L.R. Krumholz, The role of Rnf in ion gradient formation in Desulfovibrio alaskensis, PeerJ 4 (2016) e1919.
[67] M. Patón, H.H. Hernández, J. Rodríguez, Comprehensive bioenergetic evaluation of microbial pathway variants in syntrophic propionate oxidation, mSystems 5 (2020), https://doi.org/10.1128/mSystems.00814-20.
[68] N. Lindenkamp, M. Schürmann, A. Steinbüchel, A propionate CoA-transferase of Ralstonia eutropha H16 with broad substrate specificity catalyzing the CoA

thioester formation of various carboxylic acids, Appl. Microbiol. Biotechnol. 97 (2013) 7699–7709, https://doi.org/10.1007/s00253-012-4624-9.
[69] J.W. Peters, D.N. Beratan, B. Bothner, R.B. Dyer, C.S. Harwood, Z.M. Heiden, R. Hille, A.K. Jones, P.W. King, Y. Lu, C.E. Lubner, S.D. Minteer, D.W. Mulder, S. Raugei, G.J. Schut, L.C. Seefeldt, M. Tokmina-Lukaszewska, O.A. Zadvornyy, P. Zhang, M.W. Adams, A new era for electron bifurcation, Curr. Opin. Chem. Biol. 47 (2018) 32–38, https://doi.org/10.1016/j.cbpa.2018.07.026.
[70] S. Greses, N. De Bernardini, L. Treu, S. Campanaro, C. González-Fernández, Genome-centric metagenomics revealed the effect of pH on the microbiome involved in short-chain fatty acids and ethanol production, Bioresour. Technol. 377 (2023) 128920, https://doi.org/10.1016/j.biortech.2023.128920.
[71] S. Manzoor, E. Bongcam-Rudloff, A. Schnürer, B. Müller, Genome-guided analysis and whole transcriptome profiling of the mesophilic syntrophic acetate oxidising bacterium Syntrophaceticus schinkii, PLOS ONE 11 (2016) e0166520.
[72] X. Pan, I. Angelidaki, M. Alvarado-Morales, H. Liu, Y. Liu, X. Huang, G. Zhu, Methane production from formate, acetate and H2/CO2; focusing on kinetics and microbial characterization, Bioresour. Technol. 218 (2016) 796–806, https://doi.org/10.1016/j.biortech.2016.07.032.
[73] S. Dyksma, L. Jansen, C. Gallert, Syntrophic acetate oxidation replaces acetoclastic methanogenesis during thermophilic digestion of biowaste, Microbiome 8 (2020) 105, https://doi.org/10.1186/s40168-020-00862-5.
[74] N. De Bernardini, A. Basile, G. Zampieri, A. Kovalovszki, B. De Diego Diaz, E. Offer, N. Wongfaed, I. Angelidaki, P.G. Kougias, S. Campanaro, L. Treu, Integrating metagenomic binning with flux balance analysis to unravel syntrophies in anaerobic CO2 methanation, Microbiome 10 (2022) 117, https://doi.org/10.1186/s40168-022-01311-1.